01 Dec 1979

An Experimental Study Of The Reactions Of Excited Neon Atoms In Pure Afterglow Plasmas Using Resonance Absorption Spectrometry

R. A. Sierra

J. Beverley Clark
Missouri University of Science and Technology

A. J. Cunningham

Recommended Citation

R. A. Sierra et al., "An Experimental Study Of The Reactions Of Excited Neon Atoms In Pure Afterglow Plasmas Using Resonance Absorption Spectrometry," *Journal of Physics B: Atomic and Molecular Physics*, vol. 12, no. 24, pp. 4113 - 4134, article no. 17, IOP Publishing, Dec 1979.
The definitive version is available at https://doi.org/10.1088/0022-3700/12/24/017

An experimental study of the reactions of excited neon atoms in pure afterglow plasmas using resonance absorption spectrometry

J. Phys. B: Atom. Molec. Phys., Vol. 12, No. 24, 1979. Printed in Great Britain

An experimental study of the reactions of excited neon atoms in pure afterglow plasmas using resonance absorption spectrometry

R A Sierra†, J D Clark‡ and A J Cunningham‡

† Physics Department, University of Missouri at Rolla, Rolla, Missouri 65401, USA
‡ Physics Programs, University of Texas at Dallas, PO Box 688, Richardson, Texas 75080, USA

Received 14 May 1979, in final form 2 July 1979

Abstract. Resonance absorption spectrometry has been applied in a room temperature study of the reactions of excited neon atoms in pure afterglow plasmas. The pressure range 10–500 Torr was investigated. Lorentz broadened linewidths calculated using a simple classical interruption theory allowed fractional absorption signals as large as 98% to be analysed and absolute excited-state concentrations to be determined. The first absorption studies of the decay of $^1P_1$ excited atoms in neon afterglows are reported. Analysis of the decay profiles of the $^3P_2$, $^3P_0$ and $^1P_1$ excited states allowed quenching rate coefficients for each state to be determined and the role of neutral atoms and electrons in the afterglow relaxation to be studied. The importance of charge neutralisation of the dimer ion Ne_2^+ as an afterglow source of $^1P_1$ excited atoms was established in this study.

1. Introduction

With the relatively recent development of short-wavelength excimer lasers, a new importance is now attached to a detailed understanding of the quenching or de-excitation reactions of electronically excited rare-gas atoms in pulsed discharge plasmas (Lorents 1976, 1978). In this type of laser, the heavier rare gases are frequently employed as active or buffering agents and a considerable fraction of the input electrical energy delivered to the gas mixture is initially converted to energy stored on the lowest lying excited states of the rare gas used. Subsequent energy transfer reactions are used to channel this stored energy into the formation of excimer molecules and the creation of useful population inversions. Although initial attention was directed towards pure rare-gas systems, the most notable successes have been reported for rare-gas–halogen mixtures in which reactions of excited rare-gas atoms with halogen donor additives are recognised as an important reaction channel leading to the formation of the lasing rare-gas–monohalide excimer (Velazco and Setser 1975, Velazco *et al* 1976, Lorents 1978, Nigham 1978). However, despite the rapid progress which has been reported in the understanding of the kinetic processes occurring in these laser plasmas, an increasing number of excimer related studies have identified the need for a more complete data base on the reactions of the lowest lying electronically excited states of the heavier rare gases in both pure and mixed gas environments (Zamir *et al* 1976, Shaw and Jones 1977, Werner *et al* 1977, Chen *et al* 1978).

0022-3700/79/244113+22$01.00

The manifold of rare-gas excited states of particular interest in the above context is frequently referred to (Hurst and Klots 1976) as the $^3P_2$, $^3P_1$, $^3P_0$ and $^1P_1$ (Russel–Saunders notation) states and this designation will be adopted in this paper. Although only the $^3P_0$ and $^3P_2$ states are truly metastable, the $^1P_1$ and $^3P_1$ resonance levels also remain populated in high-pressure plasmas because of radiation trapping (McNeely *et al* 1975). Consequently all four of the lowest lying electronically excited states can participate in subsequent energy transfer reactions. As discussed by Golde (1977), only the reactions of the $^3P_2$ excited state of the heavier rare gases appear to have been fully characterised at present and relatively few investigations of the energy transfer reactions involving the resonance levels have been reported to date (Firestone *et al* 1979). Also, to the author's knowledge, in only one experiment has the quenching reactions of all four excited states been studied under the same operating conditions. This was in a recent study of the quenching of Ar excited states by N_2 in gas mixtures excited by an intense electron beam device (Le Calve *et al* 1977).

In response to the need identified above, we have initiated a systematic study of the de-excitation reactions of the excited states of the heavier rare gases. In this paper we present the results of a room temperature study conducted in pure neon afterglows. An extension of this work to gas mixtures is presently in progress.

The choice of neon for initial study was prompted for several reasons. Firstly, as noted by Golde, little is presently known about the reactivity of excited neon atoms in gas mixtures and, as discussed by Phelps (1959), further clarification of the destruction processes for the $^3P_0$ and $^1P_1$ states is needed for a more comprehensive overview of the energy dissipation mechanisms occurring in pure neon afterglows. Secondly, of the heavier rare gases, neon is still sufficiently small to permit completely *ab initio* calculations of the de-excitation cross sections for excited states. Indeed Cohen *et al* (1978) have recently reported the first close-coupling calculations of cross sections for neutral-induced transitions between excited neon atoms. This process is expected to play an important role in transferring population amongst excited states in the dense plasmas of interest in laser studies. The opportunity to compare experimentally measured and theoretically calculated cross sections in neon may in turn provide valuable guidance in efforts to extend the theoretical calculations to the heavier rare gases. Finally, neon is attractive from the viewpoint of experimental convenience since all four of the excited states of interest can be monitored in absorption using probing transitions lying in the accessible 5000–7000 Å spectral region.

Details of the experimental apparatus and approach are considered first in § 2. An outline of the theory used in the analysis of the absorption traces is presented in § 3, while in § 4 the salient features of the kinetic model used to obtain rate coefficients for the contributing processes are reviewed. The experimental results are presented in § 5 and discussed in § 6.

2. Experimental

The essential features of the absorption apparatus used in the present work are shown schematically in figure 1. The discharge cell was constructed from a pyrex sphere and was fitted with quartz viewing ports. Electrical breakdown of the test gas was achieved using single pulses of 10–30 kV peak voltage and 1–2 μs duration applied to a pair of internal stainless-steel disc electrodes. The interelectrode spacing used was 1·25 in and the diameter of each disc was 1·5 in. In excess of 0·6 J per pulse was delivered to the gas

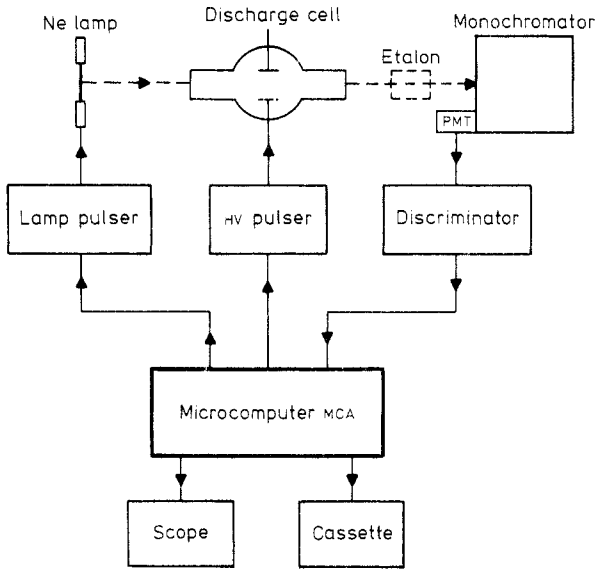

Figure 1. Schematic diagram of the absorption apparatus.

sample allowing uniform breakdown in the electrode interspace for neon pressures between 5 and 500 Torr.

Periodic high-temperature bakeout of the complete apparatus allowed evacuation to a base pressure of 10^{-9} Torr using an ion pump. A dedicated residual gas analyser (not shown) was used as a background gas monitor in the system. The test gas was introduced, via a liquid-nitrogen-cooled trap containing molecular sieve material, to the desired operating pressure and the system integrity was such that a gas sample in residence in the apparatus for a period exceeding one month showed no signs of degradation either in its emission or absorption characteristics. Visible survey spectra from the afterglow plasmas revealed the presence of neon atomic line emissions only. Fill pressures were determined using a capacitance manometer connected directly to the discharge cell.

The neon resonance lamp shown in figure 1 was of the Geissler geometry. The lamp was backfilled with neon to a pressure of approximately 5 Torr and was operated in the pulsed DC mode. Useful lamp pulse durations for this experiment varied between 3 and 15 ms for high and low (cell) pressures respectively. Resonance lines corresponding to transitions from states of the $1s^22s^22p^53p$ configuration to the $1s^22s^22p^53s$ configuration (Phelps 1959) were present in sufficient intensity from the narrow (0·5 mm ID) capillary connecting the two larger end bulbs in which the lamp electrodes were located. Resonance lines at the following wavelengths were used to monitor the neon excited states indicated; $^3P_2$ state, 6402, 6143, 6334, 5945, 5882, 6217 and 5975 Å; $^3P_1$ state, 6383, 6096, 6304, 6074 and 6030 Å; $^3P_0$ state, 6266, 6163 and 6532 Å; $^1P_1$ state, 5852 and 6599 Å. In part, the selection of these probing transitions (and the exclusion of others) was dictated by the requirement imposed by the analysis procedure outlined in § 3 that the lineshapes of the probing transitions be known. This was achieved using a confocal, piezoelectrically scanned Fabry–Perot etalon fitted with the standard red mirror set. For the 7·5 GHz free spectra range and finesse (greater than 50) of the etalon, the lineshapes for the transitions listed above were found to be Gaussian with a

slight asymmetry on the high-frequency side due to the ^{22}Ne isotope. Measured full widths at half maximum were $(2{\cdot}0 \pm 0{\cdot}2)$ GHz and no self-reversal was found for lines emitted from the central capillary zone of the lamp.

Following transit through the discharge cell, collimated output from the lamp entered a Jarrel–Ash 0·5 m monochromator. Using 25 μm entrance and exit slits the resolution of the instrument was found to be better than 1 Å allowing isolation of individual probing lines. The transmitted light was detected using a photon counting PM tube and output pulses were fed through a discriminator to a microcomputer based multichannel scaler (MCS). Count rates up to 10 MHz were found to be within the linear range of the detection and recording circuitry and the mean count rate was kept below this value (using attenuators if necessary) to avoid the need for pulse pile-up corrections. The MCS acquisition time could be varied between 1 and 255 μs per channel with no dead time. Recorded data was stored as a 16 bit signed integer in a 1021 byte buffer and could be continuously displayed in real time on an oscilloscope. Depending upon the operating pressure and probing transition used, the number of afterglow cycles required to obtain statistically meaningful signals was found to vary between 5000 and 30 000. Data collected during a data run was stored on magnetic tape for subsequent off-line analysis using a minicomputer. During data acquisition the MCS was responsible for internal generation of signals needed for operation and synchronisation of external devices such as the lamp and cell discharge circuitry. Normally the discharge was operated at twice the frequency of the lamp pulser to allow automatic subtraction (on alternate cycles) of the spontaneous emission contribution from the afterglow plasma at the probing wavelength. This capability proved to be critical in the early afterglow period when large absorption signals and hence small transmission signals were found to be typical in this work.

3. Analysis of absorption traces

A representative example of raw data collected using the apparatus described above is reproduced in figure 2. Shown is the time evolution of transmitted resonant light (5975 Å used to monitor the $^3P_2$ state) recorded in the afterglow period of a pulsed discharge in pure neon at a pressure of 188 Torr. The broken line in this plot represents the essentially constant intensity of the probing radiation recorded in the absence of an afterglow plasma. A cursory examination of figure 2 reveals that at early time almost 100% of the incident radiation was absorbed at this resonant wavelength. Similar early time behaviour was found for all resonant transitions used and throughout the pressure range investigated in this work.

The occurrence of absorption signals approaching 100% dictated the use of the analysis procedures discussed recently by Myers and Cunningham (1977). Basically this approach involved the use of the exact relationship between line absorption F $(= I_{abs}/I_{inc})$ and the lineshapes of resonant radiation and absorbing species which can be written in the integral form (Mitchell and Zeemansky 1961),

$$F = \int_{-\infty}^{\infty} E(\nu)\{1 - \exp[-k_0 l(k_\nu/k_0)]\}\,\mathrm{d}\nu \Big(\int_{-\infty}^{\infty} E(\nu)\,\mathrm{d}\nu \Big)^{-1}. \tag{1}$$

Here $E(\nu)$ denotes the lineshape of the probing radiation in the frequency interval ν to $\nu + \mathrm{d}\nu$, k_ν is the frequency-dependent absorption coefficient of the absorbing species

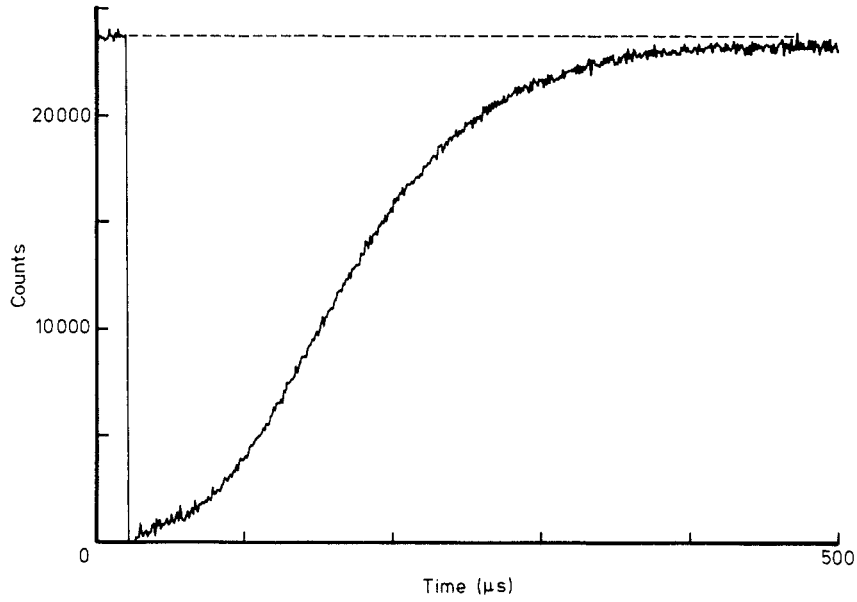

Figure 2. Typical raw data (Ne $^3P_2$ state recorded in the afterglow from a pulsed discharge in pure Ne at 188 Torr) showing 100% absorption at early time.

and k_0 is the value of k_ν at the line centre. The path length in the (assumed homogeneous) absorbing medium is denoted by l and the product $k_0 l$ is called the optical density. Of note is that k_0 is always directly proportional to absorber concentration, N, while F is only linearly proportional to k_0 and hence to N for small F values ($<20\%$) (Bemand and Clyne 1973, Davis and McFarlane 1977).

Although, in general, analytic solutions to equation (1) will not exist except in very special cases (see below), numerical solutions can be obtained provided the functional forms of $E(\nu)$ and k_ν are known. In this work the Fabry–Perot etalon was used to determine $E(\nu)$ for each probing radiation used. In the description of the lineshape of the absorber, the contributions of both Doppler and pressure broadening were incorporated as follows. The neutral gas temperature was assumed fixed at 300 K (corresponding to negligible gas heating) allowing the Doppler lineshape to be calculated (Thorne 1974). The classical theory of pressure broadening developed by Lorentz was used to calculate the influence of collisions with neutral atoms on the lineshape of the absorber (Breene 1957). In this treatment, the mean time between collisions of ground-state and excited-state atoms was required and could be estimated from diffusion data for the excited states in their parent gas (Stedman and Setser 1971). The combined Doppler and pressure broadening contributions were then described using the Voigt function which allowed the use of existing computer routines in the evaluation of (k_ν/k_0) appearing in equation (1) (Armstrong 1967). Finally, single precision arithmetic and a 40-point Gaussian quadrature formula (Abramowitz and Stegun 1970) was used to integrate equation (1) numerically to yield relationships between F and $k_0 l$ for each $E(\nu)$ and pressure studied. With this integration method numerical errors remained at least a factor of 10 smaller than the minimum detectable absorption of 0·6% attainable using the MCS.

The analysis procedure outlined above allowed F values between 98% and 0·6% to be converted to corresponding $k_0 l$ values. Above 98% small changes in F corresponded to large fluctuations in $k_0 l$ and no additional effort was undertaken to extend the reduction method to larger F values. Figure 3, shows the data of figure 2 converted to a time varying $k_0 l$ profile in this manner. Also included in this plot are $k_0 l$ profiles for the $^3P_1$ and $^3P_0$ states recorded at the same pressure of 188 Torr and processed in a similar fashion.

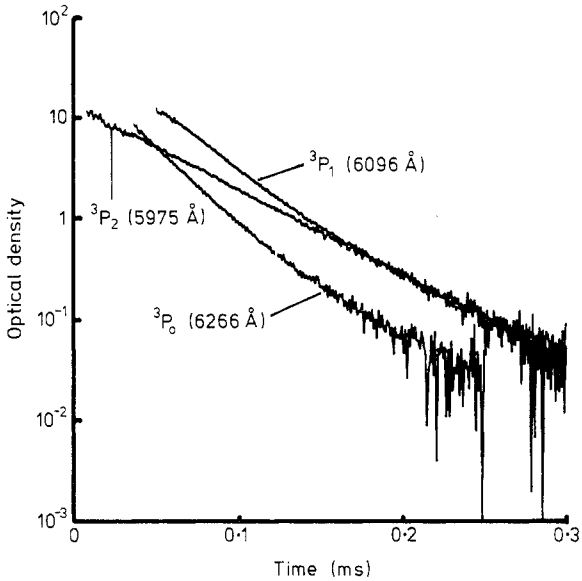

Figure 3. Time-resolved optical density plots for the triplet states at a pressure of 188 Torr.

Several consistency checks were applied to test the validity of the integration method adopted. Firstly, the optical path length was doubled by using mirrors to redirect the probing radiation for a second transit through the afterglow plasma. Under otherwise identical operating conditions, doubling the path length in this manner should yield optical density values twice those obtained upon analysis of single-pass absorption traces (Dixon and Grant 1957). For a variety of different resonant transitions and operating pressures, the observed (2 pass/1 pass) ratios were found to lie in the range 1·7 to 2·3 and showed no apparent systematic trend. Of note, however, was the observation that pairs of profiles remained parallel over the complete range of F values (98% to 0·6%) analysed. The deviations from the expected value of 2 upon doubling the path length were ultimately traced to the difficulty of maintaining identical discharge conditions throughout the long integration periods required for a complete experimental run in this study.

A second consistency check involved the use of different resonance transitions to monitor the same excited-state population decay at a given pressure. The most complete data set for this test was obtained at a pressure of 20 Torr and involved the use of all the probing transitions listed in § 2. Using tabulated values of neon oscillator strengths compiled by Wiese *et al* (1966), $k_0 l$ values (obtained using equation (1)) were converted to corresponding excited-state densities (Phelps 1959). For a given state and

operating pressure, the $k_0 l$ profiles obtained were all found to exhibit the same decay frequency throughout the range of F values analysed. However, the corresponding excited-state densities were found to exhibit a scatter of $\pm 20\%$ about a mean value. This scatter was attributed to the changing discharge conditions during the experimental run rather than to possible errors in the tabulated oscillator strengths of the neon transitions (Dixon and Grant 1957).

Although both the tests described above were generally supportive of the reduction method used, the final test involving the use of the Fabry–Perot etalon proved most conclusive. By placing the etalon in front of the monochromator as indicated by the broken lines in figure 1, the line width of the probing radiation was reduced below 100 MHz and $E(\nu)$ appearing in equation (1) could be replaced by a delta function. By virtue of the properties of this function, analytical integration of equation (1) was then possible and the fraction absorbed could be related to the optical density by the expression

$$F = 1 - \exp(-k_0 l). \tag{2}$$

Absorption data collected with the etalon in position could thus be converted directly to $k_0 l$ values without the need for numerical analysis. However, the simplification in the data reduction using the etalon was accompanied by a substantial increase in the

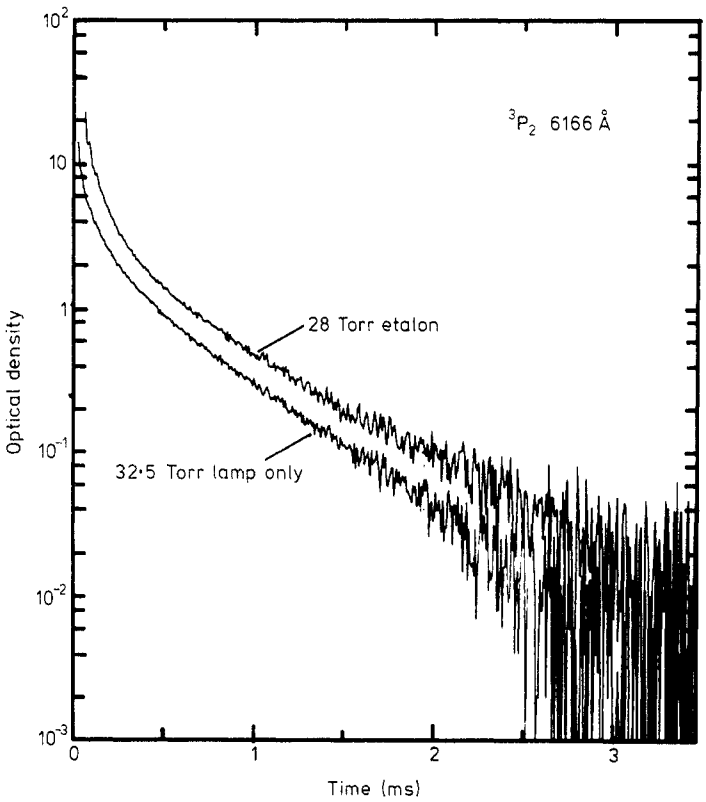

Figure 4. Comparison of $^3P_2$ state optical density profiles obtained using equation (2) (etalon) with the results of numerical analysis (equation (1)) under nearly identical operating conditions.

integration time required for the accumulation of statistically meaningful absorption traces. Typically to obtain acceptable signal-to-noise ratios, it was found necessary to average upward of 30 000 afterglow cycles. Etalon data recorded at all pressures were found to be in excellent agreement with numerically analysed data collected using the lamp only. Such a comparison is shown in figure 4 for etalon data recorded at 28 Torr and lamp-only data recorded at 32·5 Torr for the $^3P_2$ state. The results are not identical (nor should they be because of the different pressures) but clearly the general features are the same for both. Also destruction frequencies determined from optical density profiles using the etalon were found to be in excellent agreement with lamp values as illustrated by the comparisons shown in figures 5 and 7 for the $^3P_2$ and $^3P_0$ states respectively.

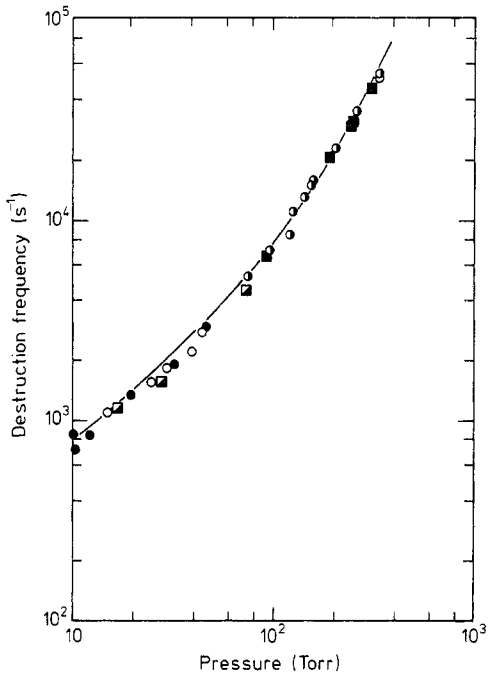

Figure 5. Plot of the measured $^3P_2$-state destruction frequency against pressure. The symbols refer to three different probing wavelengths and two different probing lineshapes. The full curve is a computer-generated fit to the data using equation (11).

Lamp only	λ (Å)	Lamp + etalon
●	5945	■
◑	5975	◪
○	6402	

The consistency checks discussed above enabled the validity of the reduction method adopted to convert raw transmission data into optical density profiles to be examined. Because of the need to analyse high fractional absorption data (at early times) special attention was directed towards the response of the numerical analysis at

large F values. The excellent agreement found between the results of the different tests lent final credence to the reduction method used.

Absolute excited-state population densities for the $^3P_2$, $^3P_1$, $^3P_0$ and $^1P_1$ states could be determined from the computed optical density profiles using tabulated values for the oscillator strengths (Wiese *et al* 1966). Knowledge of the excited-state densities for the triplet states will be required in the determination of quenching rate coefficients as discussed in § 5.

4. Kinetic model

Based primarily on the results of the comprehensive studies conducted by Phelps (1959), the afterglow decay of neon excited-state populations is expected to be controlled by the following reactions

$$M_i + Ne \underset{k_{ji}}{\overset{k_{ij}}{\rightleftharpoons}} M_j + Ne \tag{3}$$

$$M_i + 2Ne \xrightarrow{K_i} Ne_2^* + Ne \tag{4}$$

$$M_i \xrightarrow{\nu_{Ri}} Ne + h\nu \qquad (i = 1, 3) \tag{5}$$

$$M_i + e \underset{\beta_{ji}}{\overset{\beta_{ij}}{\rightleftharpoons}} M_j + e \tag{6}$$

$$M_i + M_j \xrightarrow{A_{ij}} \text{ion products.} \tag{7}$$

In this text the shorthand notation M_0, M_1, M_2 and M_3 will refer to the states $^3P_0$, $^3P_1$, $^3P_2$ and $^1P_1$ respectively and ground-state neon atoms ($^1S_0$) will be denoted by Ne. Rate coefficients are shown for each process. Not included in the above kinetic scheme are transport losses of excited states. This omission appeared to be justified since diffusion losses were calculated to remain small in comparison with other contributing processes for the experimental geometry used and pressure domain of interest in this work. To facilitate a comparison with the results of the present studies, available rate data on the individual processes are summarised below.

Previous absorption (Phelps 1959) and emission (Leichner *et al* 1975) studies conducted in decaying neon plasmas identified the reactions described by equations (3), (4) and (5) as primary loss mechanisms for excited-atom populations. In equation (3), the interconversion or mixing of excited-state populations in collisions with neon atoms is described. At room temperature, this process is expected to be very efficient since (kT/e) for neon atoms is 0·026 eV at 300 K while the energy separations of the $^3P_1$, $^3P_0$ and $^1P_1$ excited states from the lowest lying $^3P_2$ state are known to be only 0·051, 0·096 and 0·226 eV respectively. Using the principle of detailed balancing, the ratio of the excitation and de-excitation rate coefficients for equation (3) may be written in the form (Phelps 1959)

$$\eta_{ji}^0 \equiv k_{ij}/k_{ji} = (g_j/g_i)\exp(-\Delta E_{ij}/kT). \tag{8}$$

Here g denotes the degeneracy of the state, ΔE_{ij} the energy separation between states,

k is the Boltzmann constant and T the absolute temperature. From equation (8) calculated values for η^0_{12}, η^0_{02}, η^0_{01} are $8{\cdot}08\times10^{-2}$, $4{\cdot}76\times10^{-3}$ and $5{\cdot}91\times10^{-2}$, respectively, at $T=300$ K. Measured rate coefficients for equation (3) (Phelps 1959, Leichner *et al* 1975) together with calculated values reported recently by Cohen *et al* (1978) are collected in table 1. Also shown are values of the rate coefficients for the process leading to the formation of excimer molecules described in equation (4). To date values for K_i have been determined for the $^3P_2$, $^3P_1$ and $^1P_1$ states (Phelps 1959, Leichner *et al* 1975). Radiative decay of the $^3P_1$ and $^1P_1$ resonance levels is described in equation (6). Because of radiation trapping the observed lifetimes of these states greatly exceed their radiative lifetimes for the pressure domain of this work. The theory of radiation trapping developed by Holstein (1947, 1951) can be used to calculate the imprisonment decay constant ν_{Ri} but since the values obtained in this manner are geometry dependent, a comparison with other experimentally determined values is not immediately useful. Finally, electron mixing of excited-state populations and mutual ionisation of excited states are described by equations (6) and (7), respectively. Only limited experimental data for these processes in neon afterglows have been reported. This follows since in the majority of the studies conducted by Phelps, the excitation current densities used were purposely limited to minimise the importance of these channels. However for the excitation current densities employed in the present studies, which exceeded those used by Phelps by several orders of magnitude, correspondingly higher charge and excited-state densities were expected and equations (6) and (7) could not be neglected in initial modelling considerations. Phelps analysed high excitation current density data reported by Dixon and Grant (1957) to obtain an estimate of the rate coefficients for equation (6) in the case of the $^3P_0$ and $^3P_1$ states. To the authors' knowledge values of the rate coefficient A_{ij}, defined in equation (7), have not been determined for neon excited states. Unfortunately despite the larger initial excited-state densities (10^{12} cm^{-3}) produced, a direct measure of the coefficient A_{ij} was not possible in this study.

The general kinetic framework described by equations (3)–(7) proved adequate to describe the observed temporal decay of excited-state populations monitored in this work.

Table 1. Summary of rate coefficients determined in this study and comparison with previously reported values. All entries refer to 300 K.

State	Coefficient	Units	This work	Phelps (1959)	Leichner *et al* (1975)	Cohen *et al* (1978)
$^3P_2$	k_{21}	cm^3 s^{-1}	$(2{\cdot}08\pm0{\cdot}8)\times10^{-15}$	$3{\cdot}4\times10^{-15}$	5×10^{-15}	$2{\cdot}8\times10^{-15}$
	K_2	cm^6 s^{-1}	$(4{\cdot}97\pm0{\cdot}2)\times10^{-34}$	5×10^{-34}	$5{\cdot}8\times10^{-34}$	—
$^3P_0$	k_{01}	cm^3 s^{-1}	$3{\cdot}85\times10^{-15}$	5×10^{-15}	—	Small
	k_{02}	cm^3 s^{-1}	$(2{\cdot}24\pm0{\cdot}3)\times10^{-15}$	5×10^{-15}	—	$1{\cdot}3\times10^{-15}$
	β/α	—	$1{\cdot}0\pm0{\cdot}2$	$1\rightarrow2$	—	—
	K_0	cm^6 s^{-1}	$(2{\cdot}56\pm0{\cdot}14)\times10^{-34}$	7×10^{-35}	—	—
$^1P_1$	K_3	cm^6 s^{-1}	$4{\cdot}9\times10^{-33}$	—	$4{\cdot}1\times10^{-33}$	—

5. Results

What follows below are discussions of the determinations of the de-excitation rate coefficients for the $^3P_2$, $^3P_0$, $^3P_1$ and $^1P_1$ excited states of neon in their parent gas. In

agreement with the earlier studies by Phelps, it was found that the decay of the $^1P_1$ state population was sufficiently fast to be neglected in the analysis of the triplet-state profiles. Despite the extent to which the individual triplet-state populations were found to be mixed (equation (3)), the data for each excited state will be presented separately and in the order indicated above. Unless otherwise stated errors quoted on the reported rate coefficients will represent the probable errors (50% confidence level) as determined by summing the products of the residuals times the derivative of the fitting function with respect to the fitted parameter (Bevington 1969).

5.1. $^3P_2$ state

At pressures above about 100 Torr, the decay of the $^3P_2$ state population could be characterised throughout by a single exponential. This behaviour is illustrated in figure 3. At lower pressures, the onset of a late time exponential tail was found to be preceded by a period of faster decay as shown in figure 4 for two profiles recorded in the vicinity of 30 Torr. However, regardless of the operating pressure all triplet-state profiles were found to exhibit a common destruction frequency at sufficiently late time. Furthermore in this late time domain the population of the $^3P_2$ state was found to be larger than the populations of either the $^3P_1$ or $^3P_0$ states while the population of the $^1P_1$ state (see figure 9) lay below the threshold required for detection in absorption. This implies that most of the energy stored in the afterglow at late times is in the form of $^3P_2$ excited atoms with their decay controlling the afterglow relaxation.

The pressure variation of ν_2, the destruction frequency of the $^3P_2$ state (determined from the slopes of the exponential decays) is shown in figure 5. Both lamp and etalon data for three different probing transitions are seen to be in excellent agreement. The data of figure 5 can be interpreted in terms of equations (3) and (4), the two-body and three-body loss processes depending directly on neon pressure. This follows since equation (5) need not be considered for metastable states while in the late time afterglow where the exponential decay is clearly established, the reactions described by equations (6) and (7) are expected to have diminished in importance. Including only equations (3) and (4), ν_2 may be written in the form (Phelps 1959)

$$\nu_2 = -\frac{1}{[M_2]}\frac{d}{dt}[M_2] = (k_{21} - k_{12}\Pi_{12} + k_{20} - k_{02}\Pi_{02})\,[Ne] + K_2[Ne]^2. \tag{9}$$

Here the brackets [ ] denote concentrations and Π_{12} and Π_{02} define the ratios of populations in the $^3P_1$ and $^3P_0$ states relative to the $^3P_2$-state population, i.e.

$$\Pi_{12} = [M_1]/[M_2] \qquad \text{and} \qquad \Pi_{02} = [M_0]/[M_2]. \tag{10}$$

With the aid of equation (8), ν_2 may then be rewritten in the form

$$\nu_2 = k_{21}\left(1 - \frac{\Pi_{12}}{\overset{0}{\eta}_{12}}\right)[Ne] + k_{20}\left(1 - \frac{\Pi_{02}}{\overset{0}{\eta}_{02}}\right)[Ne] + K_2[Ne]^2. \tag{11}$$

Values of $\overset{0}{\eta}_{12}$ and $\overset{0}{\eta}_{02}$ can be calculated using equation (8) and the population ratios defined in equation (10) can be determined from the individual triplet-state profiles. Figure 6 shows the pressure variation of the term $\Pi_{12}/\overset{0}{\eta}_{12}$ determined from the experimental data. Because of the difficulty experienced in maintaining identical

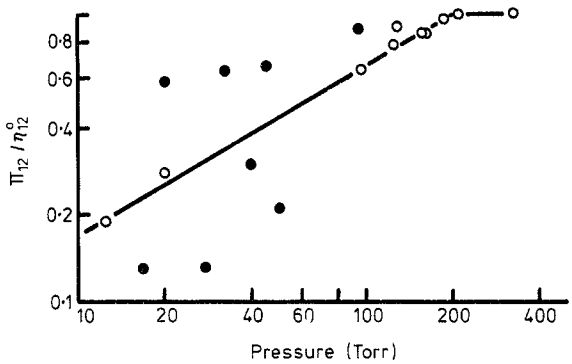

Figure 6. Ratio of $^3P_1$-state population to $^3P_2$-state population normalised to the value at thermal equilibrium (equation (8)). The open circle points correspond to data showing acceptable oscillator strength ratios (§ 5.1).

discharge conditions throughout the time period required for a complete experimental run at a given pressure, there is considerable scatter in the data shown in figure 6. It was therefore necessary to apply the following criteria as a test of the overall reliability of the Π_{12} values obtained from the experimental data. In the course of an experimental run as many as four different probing transitions were used to periodically probe the same excited-state population. Since optical density and population density are related through the value of the oscillator strength of the transition used (Phelps 1959) then at a common time in the afterglow, ratios of $k_0 l$ values, obtained using different transitions to probe the same excited-state population, should be in accordance with the ratios of the oscillator strengths (Weise *et al* 1966). If throughout the experimental run at a given pressure the observed ratios were found to be in agreement with ratios of tabulated oscillator strengths it was assumed that the Π_{12} values obtained were reliable. Data points judged to have satisfied this criterion are shown in figure 6 as open circles while those shown as full circles did not. In seeking to identify the pressure variation of Π_{12}, greater weighting was therefore given to the open circle data points. The simplest case was chosen, namely a straight line was drawn through as many of the reliable data points as possible and is shown by the full line in figure 6. The remaining data points (full circles) are seen to scatter about this line. Values of Π_{02} and $\Pi_{01}(=[M_0]/[M_1])$ could be obtained in a similar fashion.

Since the energy separation between the $^3P_2$ and $^3P_0$ states in neon is approximately twice that between the $^3P_2$ and $^3P_1$ states, the second term on the right-hand side of equation (11) is expected to remain smaller than the first. This was confirmed by comparing the magnitudes of the coefficients k_{21} and k_{20} (obtained from k_{02} using equation (8)) which showed the term involving k_{20} to be negligible. Retaining only the first and third terms in equation (11) and using the pressure variation for Π_{12}/η^0_{12} shown in figure 6, the expression for ν_2 could be fitted to the data of figure 5. The full line drawn through the data points is a result of the least-squares fitting. The rate constants obtained from the fitting procedure were

$$k_{21} = (2{\cdot}08 \pm 0{\cdot}08) \times 10^{-15}\ \text{cm}^3\ \text{s}^{-1} \tag{12}$$

and

$$K_2 = (4{\cdot}97 \pm 0{\cdot}2) \times 10^{-34}\ \text{cm}^6\ \text{s}^{-1}. \tag{13}$$

5.2. $^3P_0$ state

Inspection of the decay profile of the $^3P_0$ state shown in figure 3 reveals the presence of an early time fast exponential decay which persists for approximately one order of magnitude in optical density. At late time the decay of the $^3P_0$ state is seen to be controlled by the decay of the $^3P_2$ state. These are high pressure (greater than 100 Torr) characteristics. At lower pressures a unique early time exponential region could not be identified and was replaced by a gradual transition from the early time fast decay to the later time $^3P_2$-state-controlled exponential decay. This low-pressure data will be considered later in an attempt to evaluate the role of electron mixing collisions described by equation (6).

All the data for which early time logarithmic destruction frequencies could be identified are plotted in figure 7. Again lamp and etalon data are seen to be in good agreement. Following the same approach as presented in § 5.1, the decay constant for $^3P_0$ state can be expressed in the form

$$\nu_0 = k_{01}\left(1-\frac{\eta^0_{01}}{\Pi_{01}}\right)[\mathrm{Ne}]+k_{02}\left(1-\frac{\eta^0_{02}}{\Pi_{02}}\right)[\mathrm{Ne}]+K_0[\mathrm{Ne}]^2. \tag{14}$$

For pressures in the range 100–500 Torr, values for Π_{01} and Π_{02} appearing in equation (14) could be determined from the data. The term η^0_{02}/Π_{02} was found to be much less than unity throughout and could be neglected while η^0_{01}/Π_{01} had an essentially constant

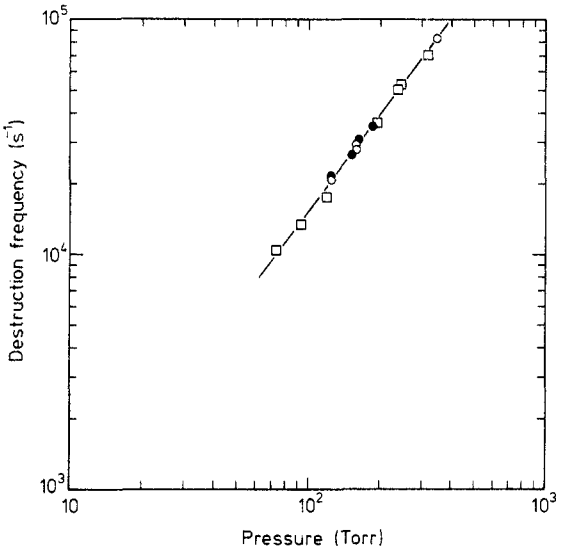

Figure 7. Plot of the measured $^3P_0$-state destruction frequency against pressure. The symbols refer to different probing wavelengths and line widths. The full line is a computer-generated fit to the data using equation (15).

Lamp only	λ (Å)	Lamp + etalon
●	6163	
○	6266	□

value of 0·3. Substituting back into equation (14), the data of figure 7 could then be fitted to an expression of the form

$$\nu_0 = (0{\cdot}7k_{01} + k_{02})[\mathrm{Ne}] + K_0[\mathrm{Ne}]^2. \tag{15}$$

The solid line shown in figure 7 is a least-squares fit to the data. The values of the coefficients obtained were

$$(0{\cdot}7k_{01} + k_{02}) = (4{\cdot}94 \pm 0{\cdot}30) \times 10^{-15}\ \mathrm{cm}^3\ \mathrm{s}^{-1} \tag{16}$$

and

$$K_0 = (2{\cdot}56 \pm 0{\cdot}14) \times 10^{-34}\ \mathrm{cm}^6\ \mathrm{s}^{-1}. \tag{17}$$

As discussed in § 5.3 an independent determination of k_{01} was possible allowing a value for k_{02} to be established.

For operating pressures less than 100 Torr the early time non-exponential decay of the $^3P_0$ excited-atom population could not be interpreted in terms of the collisional processes described by equations (3) and (4) alone. The role of the additional loss processes described by equations (6) and (7) were considered and as discussed below, the inclusion of equation (6) together with the intrinsic loss processes depending on neon pressure provided a satisfactory description of this early time data. This analysis was greatly facilitated by the observation that in the early time decay, the terms Π_{01}/η^0_{02} and Π_{02}/η^0_{02} greatly exceeded unity implying that the $^3P_0$ excited-atom population decayed independently of the other triplet-state populations. Source terms from the $^3P_2$ and $^3P_1$ excited states could then be neglected and the differential equation governing the decay of the $^3P_0$-state population could be solved to obtain an early time solution of the form

$$[\mathrm{M}_0](t) = [\mathrm{M}_0](t=0)\exp\left(-\nu_0 t - \int_0^t \beta[\mathrm{e}]\right) \mathrm{d}t \tag{18}$$

where ν_0 is already defined in equation (15) as a sum of two-body and three-body terms. The term involving β includes the sum of appropriate loss terms describing quenching by electrons, i.e.

$$\beta = \beta_{01} + \beta_{02}. \tag{19}$$

In order to make use of equation (18) to fit the early time $^3P_0$-state data, knowledge of the time evolution of electron density is required. Unfortunately this parameter was not specifically monitored in this work and it was necessary to assume that the electron density decay was controlled by the fast electron–ion dissociative recombination of the dimer ion Ne_2^+ (Bardsley and Biondi 1970). As discussed in § 5.4, for the operating pressures of this study atomic neon ions produced during the discharged pulse will be rapidly converted to the dimer ion Ne_2^+. Under conditions of charge neutrality and the assumption that the afterglow plasmas contain a single ion species, Ne_2^+, the electron density decay can be obtained from the 'recombination solution' as

$$[\mathrm{e}](t) = [\mathrm{e}](t=0)/(\alpha[\mathrm{e}](t=0) + 1) \tag{20}$$

where α denotes the dissociative-recombination rate coefficient. For Ne_2^+, α has a well established value of $2 \times 10^{-7}\ \mathrm{cm}^3\ \mathrm{s}^{-1}$ at 300 K (Bardsley and Biondi 1970). With the aid

of equation (20) it is then possible to evaluate equation (18) to obtain an early time solution of the $^3P_0$ excited-state population decay of the form

$$[M_0](t) = [M_0](t=0)\exp(-\nu_0 t)(\nu_e t + 1)^{-\beta/\alpha} \tag{21}$$

where

$$\nu_e = \alpha[e](t=0). \tag{22}$$

Using a non-linear least-squares fitting procedure (Marquardt 1963), equation (21) was then used to fit the early time $^3P_0$ data with the time $t = 0$ set arbitrarily at approximately 100 μs into the afterglow decay. The quality of the resultant fits was impressive and values of β/α for two probing transitions are plotted as a function of pressure in figure 8.

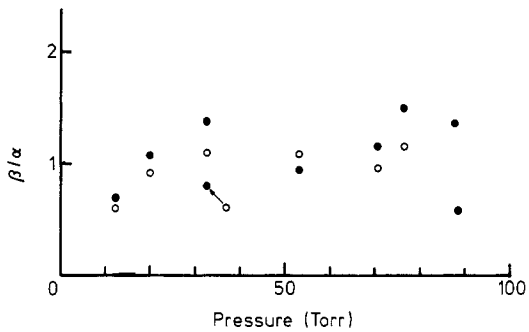

Figure 8. Ratio of the total superelastic de-excitation rate coefficient (β) for the $^3P_0$ state to the dissociative recombination rate coefficient of the dimer ion Ne_2^+ at various pressures and two different probing wavelengths: ○ 6163 Å, ● 6266 Å.

The average value of the ratio β/α obtained from this plot was $1{\cdot}0 \pm 0{\cdot}2$ with the error representing the probable error (two thirds of the standard deviation) as determined from scatter about the mean. Although disturbing, the large error is understandable since the fitted parameters, $[M_0](t=0)$, ν_e, ν_0 and β/α, are strongly correlated making the fitting process difficult. The validity of the results obtained can be judged by comparing the fitted value of ν_0 with that obtained using equation (15). Worst-case errors of less than 50% were observed for this parameter which again seemed acceptable in the light of the difficult nature of the fitting procedure necessary.

From the values of ν_e obtained in the fitting process, the electron density at the initial point ($t = 100$ μs) was found to be about 4×10^{10} cm^{-3}. However, if extrapolation was used to obtain the electron density immediately following the termination of the excitation pulse, negative values were implied. Possible explanations of this result include either that there exists a decaying source term for electrons (such as equation (7)) which has not been incorporated into equation (18) or, as suggested by an unidentified referee, that the electron temperature had not yet fully relaxed in the early afterglow decay (Dean *et al* 1974). In the latter case the presence of an elevated electron temperature would result in a lower initial value of α (Bardsley and Biondi 1970) which would also mimic the extrapolated result. Unfortunately, it was not possible with our data base to distinguish between these possible explanations at this time.

5.3. $^3P_1$ state

Inspection of figure 3 suggests a close correlation between the decays of the $^3P_1$ and $^3P_0$ atom populations in the early afterglow period while all triplet-state populations are seen to decay with a common destruction frequency (ν_2) at sufficiently late time. It was found that for pressures exceeding 100 Torr all triplet-state profiles could be accurately represented using a sum of two exponentials of the form (Leichner *et al* 1975)

$$[M](t) = A_0 \exp(-\nu_0 t) + A_2 \exp(-\nu_2 t) \tag{23}$$

where A_0 and A_2 are constants to be determined by fitting and ν_2 and ν_0 are defined in equations (9) and (14) and are plotted in figures 5 and 7 respectively.

The ability to describe the decay of the $^3P_1$-state population using terms depending only on the decay constants ν_0 and ν_2 implies that source terms control the afterglow evolution of the $^3P_1$-state population. This interpretation could be confirmed by inspection of the differential equation describing the decay of population in this state

$$\frac{d}{dt}[M_1] = -(\nu_{R1} + \nu_1)[M_1] + (k_{01}[M_0] + k_{21}[M_2])[Ne]. \tag{24}$$

Here ν_{R1} denotes the inverse of the effective radiative lifetime of the $^3P_1$ state and includes the role of multiple absorption and re-emission of resonant radiation (Holstein 1947, 1951). Although not evaluated for the specific cell geometry used in this work, an order of magnitude estimate of 10^4 s^{-1} for ν_{R1} was obtained by assuming an equivalennt spherical geometry (of radius equal to the inter-electrode spacing) and using the calculations of Holstein applied to cylindrical geometries. The destruction frequency ν_1 includes collisional loss due to equations (3) and (4) and may be written as

$$\nu_1 = (k_{10} + k_{12})[Ne] + K_1[Ne]^2. \tag{25}$$

The remaining term in equation (24) describes the production of $^3P_1$ excited atoms in collisional de-excitation of the metastable $^3P_0$ and $^3P_2$ excited states. Using values of the appropriate rate coefficients from table 1, the source terms in equation (24) were found to control the decay rate of $^3P_1$ excited-atom population. Because of this it was not possible to derive $^3P_1$ quenching rate data by fitting to the decay profiles of this state.

However, from the values of the A_2 coefficient obtained on fitting the $^3P_0$ and $^3P_1$ profiles using equation (23) it was possible to obtain improved estimates for k_{01} and k_{02} as follows. Since in the late time decay all triplet-state profiles show the same exponential destruction frequency, ν_2, the first term in equation (23) can be neglected in this time domain and the ratio of the A_2 coefficients obtained for the $^3P_0$ and $^3P_1$ states then provides a value for Π_{01}. In the late time period the term η^0_{02}/Π_{02} was found to be unity for pressures exceeding 100 Torr allowing equation (14) to be rewritten as

$$\nu_0 = \nu_2 = 0{\cdot}38\, k_{01}[Ne] + K_0[Ne]^2. \tag{26}$$

Adopting the value of K_0 given in equation (17) and values of ν_2 from figure 5 allowed equation (26) to be solved to obtain a value for k_{01}. From three high-pressure data runs the value obtained was

$$k_{01} = 3{\cdot}85 \times 10^{-15}\ \text{cm}^3\ \text{s}^{-1}. \tag{27}$$

It must be stressed, however, that this analysis could only be applied to the limited high-pressure range of 170–200 Torr when $\Pi_{12} \neq \eta^0_{12}$ and where reliable values of Π_{12} were available (see figure 6).

From equation (16) the value

$$k_{02} = (2{\cdot}24 \pm 0{\cdot}3) \times 10^{-15} \text{ cm}^3 \text{ s}^{-1} \tag{28}$$

was then determined.

5.4. $^1P_1$ state

Representative low (12·5 Torr) and high (188 Torr) pressure decay profiles for the $^1P_1$ excited state are shown in figure 9. These profiles show a reversal in the pressure trend observed in the study of the triplet states (i.e. single exponential decays at low rather than high pressure). Also noted is the recognisable build up in population of the $^1P_1$ state immediately following the termination of the excitation pulse which was not evident in any triplet-state profiles. These differences suggest that the decay of the $^1P_1$ state may be controlled by processes other than those governing the disappearance of the triplet-state populations. Furthermore adopting the same approach as followed in § 5.3, the results of the calculations presented by Holstein were used to estimate the magnitude of the inverse effective radiation lifetime of the $^1P_1$ state and a value of approximately 7 μs was obtained for ν_{R3}. On this basis, rapid radiative depletion of the $^1P_1$-state population was expected but as shown in the profiles plotted in figure 9 a significant population of this state was found at late time. When the observed build up in $^1P_1$-state population is also considered it must be concluded that source terms play an important role in the decay of this state.

A potential afterglow source of $^1P_1$ excited atoms has been identified by Frommhold and Biondi (1969). In studies of decaying plasmas in pure neon, a number of neutral neon emissions, including a prominent feature at 5852 Å, were observed to result from the electron–ion dissociative recombination of the dimer ion Ne_2^+. In pure afterglows

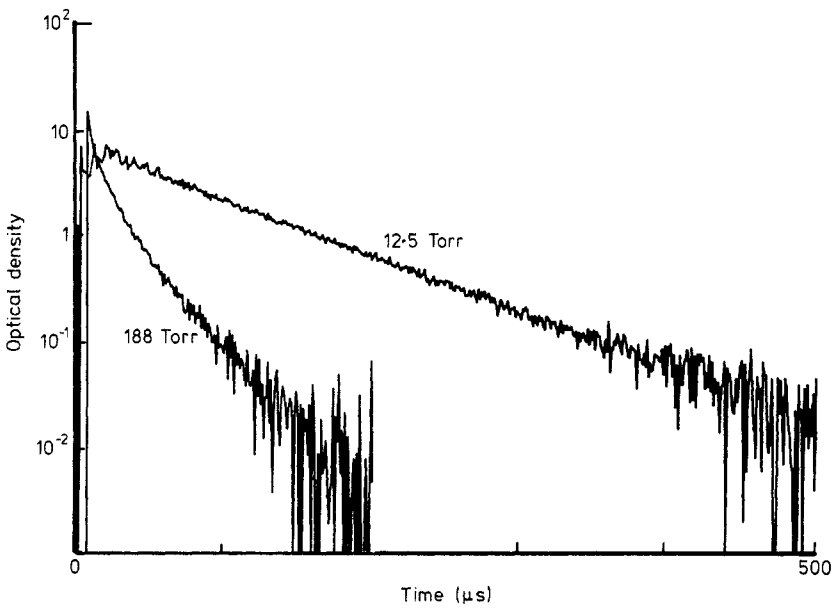

Figure 9. Optical density decay profiles for the $^1P_1$ state obtained using the 5852 Å probing transition at pressures of 12·5 and 188 Torr.

this ion is known to be formed in the fast association reaction

$$Ne^+ + 2Ne \xrightarrow{K^+} Ne_2^+ + Ne. \tag{29}$$

K^+, the rate coefficient for this reaction, has been reported to be in the range $(5\text{–}8)\times 10^{-32}$ cm^6 s^{-1} (Vitol and Oskam 1972) allowing the rate of dimer–ion production, $K^+[Ne]^2$, to be calculated.

Recalling that the results of § 5.2 suggest a value of 4×10^{10} cm^{-3} after 100 μs, the electron density immediately following the termination of the discharge pulse can be estimated to exceed 10^{11} cm^{-3}. The rate of dimer-ion density decay and hence production of $^1P_1$ atoms by recombination is given by $\alpha[e]$ (see below). For pressures less than about 20 Torr, $\alpha[e]$ is greater than $K^+[Ne]^2$ and this implies that low-pressure $^1P_1$-state decay profiles will reflect the rate of dimer–ion production described by equation (29) which indicates an exponential decay for the parent Ne^+ ion. Three data runs at pressures of 12·5, 17 and 20 Torr showed an exponential decay of the $^1P_1$-state population (see figure 9). The average decay constant from these three runs was

$$K^+ = 6{\cdot}3\times 10^{-32}\ \text{cm}^6\ \text{s}^{-1} \tag{30}$$

which is in excellent agreement with the literature value of this coefficient.

The analysis of the non-exponential decays observed at pressures exceeding 20 Torr was not as straightforward since the recombination step becomes rate limiting. The differential equation describing the disappearance of the $^1P_1$-state population may be written as

$$\frac{d}{dt}[M_3] = -\nu_3[M_2] + \alpha_P[e][Ne_2^+] \tag{31}$$

where ν_3 denotes the combined radiative and collisional loss of this state and α_p represents the partial recombination rate coefficient and corresponds to the fraction of recombination events in which $^1P_1$ excited atoms are produced. The electron density decay can be written in the form

$$\frac{d}{dt}[e] = -\alpha[e][Ne_2^+] + A[M_i][M_j]. \tag{32}$$

Here the source term accounts for the production of electrons in mutual ionising collisions described by equation (7). Unfortunately, useful solutions to equations (31) and (32) could not be obtained and another approach was indicated for the analysis of the $^1P_1$ data at higher pressures. It was found that for pressures exceeding 50 Torr the decay of the $^1P_1$-state populations could be represented by a sum of two exponentials

$$[M_3](t) = A_3\exp(-\nu_3 t) + A_4\exp(-\nu_4 t) \tag{33}$$

and that the values of ν_3 determined by computer fitting were a factor of 6 larger than ν_4 at all pressures. Values of the fast decay component obtained in this manner are plotted in figure 10. Both a pressure-independent term and a three-body term were required to fit the data of this plot suggesting that radiative decay (equation (5)) and the three-body process described in equation (4) are primary loss processes for this excited-atom population. The solid line in figure 10 is a least-squares fit using the expression

$$\nu_3 = \nu_{R3} + K_3[Ne]^2. \tag{34}$$

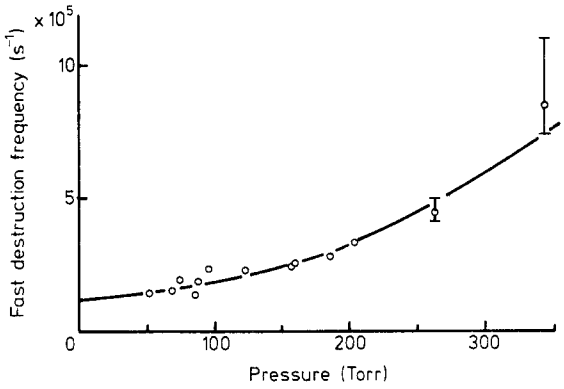

Figure 10. Plot of the fast destruction frequency (ν_3) for the $^1P_1$ state at various pressures. The solid line is a computer generated fit to data using equation (34).

The values of ν_{R3} and K_3 determined by fitting were

$$\nu_{R3} = 1{\cdot}33 \times 10^5 \text{ s}^{-1} \tag{35}$$

and

$$K_3 = 4{\cdot}9 \times 10^{-33} \text{ cm}^6 \text{ s}^{-1}. \tag{36}$$

Values of the slow decay component (ν_4), which attempts to describe the time varying recombination source term in equation (31), were found to be grouped about $(3{\cdot}5\text{–}5) \times 10^4 \text{ s}^{-1}$ and exhibited little if any pressure dependence. However, in lieu of more specific information on the electron density decay, further interpretation of this slow decay component could not be attempted and this term was relegated to the status of background and was not included further in the kinetic analysis at this time.

6. Discussion and summary

The results of the present investigations have confirmed the conclusions reached by previous workers (Phelps 1959, Leichner *et al* 1975) that collisions with ground-state neon atoms play a central role in the relaxation of excited-atom populations in pure afterglow plasmas. With the notable exception of the $^3P_1$ excited state, contributions of either or both the two-body and three-body processes described by equations (3) and (4), respectively, could be identified and appropriate rate coefficients determined. Examination of early time $^3P_0$-state data indicated the importance of mixing collisions with electrons described in equation (6). Finally, analysis of the $^1P_1$-state decay profiles served to highlight the importance of the charge neutralisation of the dimer ion Ne_2^+ as an afterglow source of $^1P_1$ excited atoms for the operating conditions of the present study.

Comparisons of the various rate coefficients determined in this work with values reported by other workers are shown in table 1. All entries refer to 300 K. Our values of the rate coefficients K_2 and K_1 are seen to be in good agreement with values reported by Phelps (1959) (in absorption studies) and Leichner *et al* (1975) (in emission studies). The value reported here for K_0 is, however, seen to be a factor of thirty larger than that obtained by Phelps. Our larger value for this coefficient might be preferred since the

value reported by Phelps was obtained from the analysis of a single data point and could be considered suspect for this reason.

Although the magnitudes of the bimolecular rate coefficients for equation (3) determined in this work are seen to be in general agreement with those reported previously, our values are seen to be systematically lower. As discussed in § 5, the accurate determination of the population ratios Π_{01}, Π_{02}, etc, is of critical importance in this context. In this investigation absolute, as distinct from relative population densities for each of the lowest lying excited states, could be determined from recorded absorption traces using equation (1). Furthermore, as discussed in § 3, fractional absorption traces as large as 98% could be analysed without the need to use empirical relationships between fractional absorption and optical density. Nevertheless, difficulties were experienced in maintaining identical discharge conditions at the large current density employed in this work. This rendered an accurate determination of the population density ratios difficult and whether this may account for the lower values reported here for the coefficients k_{01} and k_{02} is not clear at this time and will be explored in future studies. The overall disagreement between theory and experiment in the case of k_{01} and k_{02} is not considered to be serious at this time since in the calculations of Cohen *et al* (1978) angular coupling was neglected and when included is expected to yield larger calculated values for these coefficients (J S Cohen, private communication).

From the data of figure 9, a value of $1{\cdot}0 \pm 0{\cdot}2$ was determined for (β/α) in the case of the $^3P_0$ state. Phelps (1959) analysed low-pressure data obtained by Dixon and Grant (1957) and found that $1 \leqslant (\beta/\alpha) \leqslant 2$. The approach used by Phelps was to change the differential equation describing the decay of the $^3P_0$ state population into a difference equation and make use of available data to invert the resulting set of normal equations. Due to noise in the data, such an approach will almost invariably be dealing with a nearly singular set of equations and will introduce significant scatter in the results. The value obtained for β/α by the more direct approach followed in this work might then be considered to be more reliable. Unfortunately, it was not possible to extend the analysis outlined in § 5.2 to obtain values of the β coefficients for the $^3P_2$ and $^3P_1$ excited states since the assumption of an early time-independent decay was not valid for these states. The already complex analysis would have rapidly become intractable and in lieu of an independent-electron density measurement was not pursued further at this time.

The large discharge current densities employed in this work did, however, allow the first absorption studies of the decay of $^1P_1$ excited-atom populations in pure neon afterglows. Previously this state had been studied in emission only (Leichner *et al* 1975). The salient features of the decay profiles for this state could be described using the recombination based model presented in § 5.4. At low pressures the decay of the $^1P_1$-state population was found to be controlled by the rate of conversion of Ne^+ to Ne_2^+. For pressures exceeding 50 Torr the recombination of Ne_2^+ and electrons became the rate limiting step and the decay could be described as the sum of two exponentials. The fast decay component could be interpreted to represent the combined collisional and radiative decay of the $^1P_1$ excited-atom population and the value of the pressure-independent component was found to be consistent with the value of ν_{R3}, the imprisonment decay constant for this state, calculated using Holstein's theory. Although this agreement is considered encouraging, the need to use an approximate description of the cell geometry to calculate ν_{R3} suggests caution in drawing any additional inferences concerning the agreement between the results of Holstein's theory and this experiment. However, our value of the three-body rate coefficient, K_3, is seen to be in excellent agreement with the value reported by Leichner *et al* (1975).

Finally, in future studies it is planned to continue to exploit the technique of resonance absorption spectrometry to further investigate and, hopefully, elucidate several poorly understood aspects of the competition amongst the various reaction channels involving neon excited-atom populations in both pure and mixed gas afterglow plasmas. For example, it is planned to investigate both the temperature dependence and branching ratios of the processes identified in this study. A preliminary survey has already confirmed the presence of a small absorption signal in the vicinity of 8150 Å which has been ascribed to an absorption band of the Ne_2 excimer molecule (Arai *et al* 1978). An extension of these preliminary studies will permit an investigation of the specific atomic excited states leading to the formation of excimer molecules in equation (4) and whether such reactions are occurring on attractive or repulsive portions of potential surfaces (Golde 1977). Both the knowledge of absolute excited-atom populations and the proven ability to monitor the contribution of each excited state will greatly facilitate these studies.

Acknowledgments

The authors wish to acknowledge the assistance of Dr G Myers in the acquisition and reduction of the absorption data and the financial support provided by the University of Texas at Dallas' Organized Research Funds under which much of this work was carried out.

References

Abramowitz M and Stegun I A 1970 *Handbook of Mathematical Functions* (Washington, DC: NBS)
Armstrong B H 1967 *J. Quant. Spectrosc. Radiat. Transfer* **7** 61–88
Arai S, Oka T, Kogoma M and Imamura M 1978 *J. Chem. Phys.* **68** 4595–603
Bardsley J N and Biondi M A 1970 *Advances in Atomic and Molecular Physics* ed D R Bates and I Estermann, vol 6 (New York: Academic) pp 1–57
Bemand P P and Clyne M A A 1973 *J. Chem. Soc. Faraday Trans. II* **69** 1643–57
Bevington P R 1969 *Data Reduction and Error Analysis for the Physical Sciences* (New York: McGraw-Hill)
Breene R G 1957 *Rev. Mod. Phys.* **29** 94–143
Chen C H, Payne M G and Judish J P 1978 *J. Chem. Phys.* **69** 1626–35.
Cohen J S, Collins L A and Lane N F 1978 *Phys. Rev.* A **17** 1343–56
Davis C C and McFarlane R A 1977 *J. Quant. Spectrosc. Radiat. Transfer* **18** 151–70
Dean A G, Smith D and Adams N G 1974 *J. Phys. B: Atom. Molec. Phys.* **7** 644–56
Dixon J R and Grant F A 1957 *Phys. Rev.* **107** 118–24
Firestone R F, Oka T and Takao S 1979 *J. Chem. Phys.* **70** 123–30
Frommhold L and Biondi M A 1969 *Phys. Rev.* **185** 244–52
Golde M F 1977 *Gas Kinetics and Energy Transfer* ed P G Ashmore and R J Donovan, vol 2 (London: Chemical Society) pp 123–74
Holstein T 1947 *Phys. Rev.* **72** 1212–33
—— 1951 *Phys. Rev.* **83** 1159–68
Hurst G S and Klots C E 1976 *Advances in Radiation Chemistry* ed M Burton and J L Magee, vol 5 (New York: Wiley) pp 1–96
Le Calve J, Gutcheck R A and Dutuit O 1977 *Chem. Phys. Lett.* **47** 470–4
Leichner P K, Cook J D and Luerman S J 1975 *Phys. Rev.* A **12** 2501–13
Lorents D C 1976 *Physica C* **82** 19–26
—— 1978 *Electronic and Atomic Collisions* ed G Watel (Amsterdam: North-Holland) pp 663–79
McNeely J R, Hurst G S, Wagner E B and Payne M G 1975 *J. Chem. Phys.* **63** 2717–23
Marquardt D W 1963 *J. Soc. Ind. Appl. Math.* **11** 431–41

Mitchell A C G and Zemansky M W 1961 *Resonance Radiation and Excited Atoms* (London: Cambridge University Press) chap 3, 4
Myers G and Cunningham A J 1977 *J. Chem. Phys.* **67** 247–53
Nigham W L 1978 *IEEE J. Quantum Electron.* **QE-14** 714–26
Phelps A V 1959 *Phys. Rev.* **114** 1011–25
Shaw M J and Jones J D C 1977 *Appl. Phys.* **14** 393–8
Stedman D H and Setser D W 1971 *Prog. React. Kinet.* **6** 193–238
Thorne A P 1974 *Spectrophysics* (New York: Wiley) chap 8, 9
Velazco J E, Kolts J H and Setser D W 1976 *J. Chem. Phys.* **65** 3468–80
Velazco J E and Setser D W 1975 *IEEE J. Quantum Electron.* **11** 708–9
Vitol A and Oskam J 1972 *Phys. Rev.* A **5** 2618–22
Werner C W, George E V, Hoff P W and Rhodes C K 1977 *IEEE J. Quantum Electron.* **QE-13** 769–83
Wiese W L, Smith M W and Glennon B M 1966 *Atomic Transition Probabilities* NSRDS-NBS4, vol 1 (Washington, DC: US Govt Printing Office)
Zamir E, Szöke A and Osgood R (1976) *J. Chem. Phys.* **65** 4885–94